JACS
JOURNAL OF THE AMERICAN CHEMICAL SOCIETY
pubs.acs.org/JACS
Article

Topology-Accelerated and Selective Cascade Depolymerization of Architecturally Complex Polyesters

Changxia Shi, Nicholas A. Rorrer, Alexander L. Shaw, Ryan W. Clarke, Bonnie L. Buss, Gregg T. Beckham, Linda J. Broadbelt,* and Eugene Y.-X. Chen*

Cite This: J. Am. Chem. Soc. 2024, 146, 9261−9271
Read Online

ABSTRACT: Despite considerable recent advances already made in developing chemically circular polymers (CPs), the current framework predominantly focuses on CPs with linear-chain structures of different monomer types. As polymer properties are determined by not only composition but also topology, manipulating the topology of the single-monomer-based CP systems from linear-chain structures to architecturally complex polymers could potentially modulate the resulting polymer properties without changing the chemical composition, thereby advancing the concept of monomaterial product design. To that end, here, we introduce a chemically circular hyperbranched polyester (HBPE), synthesized by a mixed chain-growth and step-growth polymerization of a rationally designed bicyclic lactone with a pendent hydroxyl group (BiL^{OH}). This HBPE exhibits full chemical recyclability despite its architectural complexity, showing quantitative selectivity for regeneration of BiL^{OH}, via a unique cascade depolymerization mechanism. Moreover, distinct differences in materials properties and performance arising from topological variations between HBPE, *hb*-PBiL^{OH}, and its linear analogue, *l*-PBiL^{OH}, have been revealed where generally the branched structure led to more favorable interchain interactions, and topology-amplified optical activity has also been observed for chiral (1*S*, 4*S*, 5*S*)-*hb*-PBiL^{OH}. More intriguingly, depolymerization of *l*-PBiL^{OH} proceeds through an unexpected, initial topological transformation to the HBPE polymer, followed by the faster cascade depolymerization pathway adopted by *hb*-PBiL^{OH}. Overall, these results demonstrate that CP design can go beyond typical linear polymers, and rationally redesigned, architecturally complex polymers for their unique properties may synergistically impart advantages in topology-augmented depolymerization acceleration and selectivity for exclusive monomer regeneration.

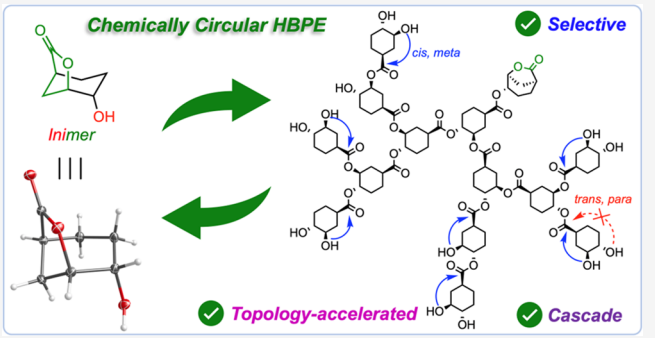

INTRODUCTION

Polymeric materials, despite being ubiquitous and indispensable in our daily life and the global economy, are facing mounting environmental pollution, societal outcry, and regulatory pressure.[1−6] Developing a circular materials economy[7−9] is arguably the most effective solution to address these issues, by endowing polymers with intrinsic chemical recyclability[10]—circular polymers (CPs) with closed-loop circularity, through design of new monomers/polymers, catalysts, and (de)polymerization methods.[11−18] As part of this effort, increasing innovations in synthetic polymer chemistry have continuously created numerous strategies for producing polymer materials with tailored properties and functionalities.[19−21] It is well-known that the properties of polymers are determined not only by their composition (i.e., the types of monomers employed in their synthesis) but also by their topology. Variations in the way polymer chains interconnect can result in distinct material properties for polymers composed of the same monomer. Consequently, manipulating the topology of a single-polymer composition significantly influences the properties of the resulting polymer, yielding characteristics unattainable in the case of linear polymers.[22−26] For instance, linear high-density polyethylene is stiff and strong and is used in high-strength applications such as bullet-proof vests, whereas branched low-density polyethylene is flexible and used in softer applications such as plastic films. In this way, various polymer architectures have been developed,[27] including linear, cyclic,[28,29] branched,[30−36] and cross-linked topologies,[37−40] meeting the growing and diverse application demands.

Among the diverse topological polymers, hyperbranched polymers, including hyperbranched polyesters (HBPEs), have garnered considerable interest due to their distinctive 3D

Received: January 16, 2024
Revised: March 9, 2024
Accepted: March 11, 2024
Published: March 22, 2024

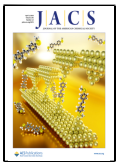

https://doi.org/10.1021/jacs.4c00526
J. Am. Chem. Soc. 2024, 146, 9261−9271

Scheme 1. Inimer (*Ini*tiator and Mono*mer*) BiL^{OH} and Proposed Mixed "Chain-Growth" and "Step-Growth" Mechanism for Accessing Chemically Recyclable *hb*-PBiL^{OH}

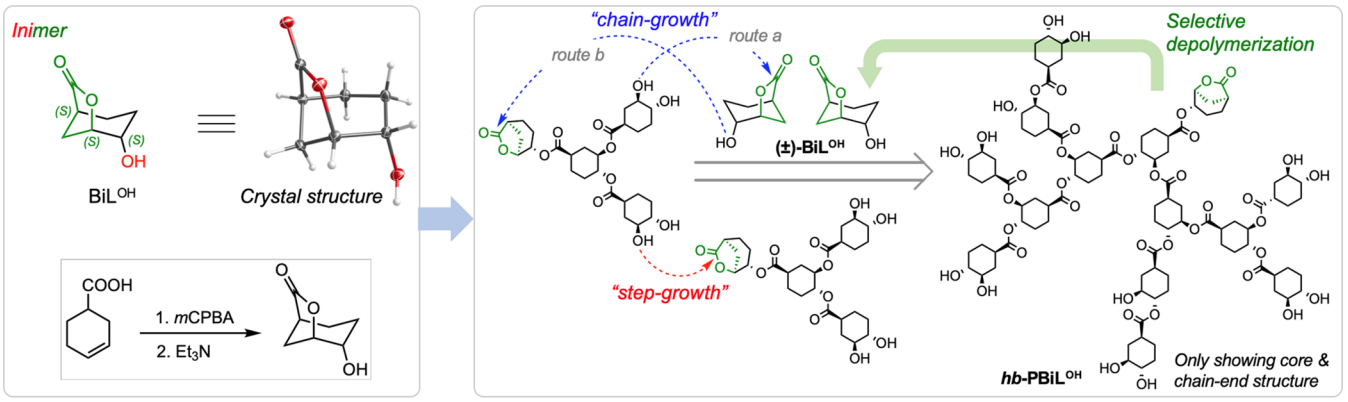

globular structures, intriguing physical and chemical properties, and abundant functional end groups.[30−36,41−44] Unlike their perfectly symmetrical counterparts, dendrimers,[45,46] hyperbranched polymers can be produced on a commercially viable scale using a streamlined one-step process while preserving key features of dendrimers, such as excellent solubility, low solution/melt viscosity (which facilitates processing), and a high degree of functionality. These attributes render them appealing for various biological applications such as drug delivery, tissue engineering, and bioimaging.[33−36,47] Furthermore, branching is a pervasive and crucial phenomenon that can lead to accelerated, more efficient transfer, dissipation, and distribution of energy or matter.[30]

Current research on CPs predominantly focuses on linear polymers.[7−10] The challenge of efficiently and selectively depolymerizing intricate, highly functionalized, and architecturally complex polymers such as HBPE remains underexplored. While several exemplary chemically recyclable brush polymers have been reported, these instances mainly rely on the recyclability of the backbone, resulting in depolymerization products that are still polymers with reduced molecular mass.[48,49] Thus, to render architecturally complex polymers with full chemical recyclability toward a circular materials economy, innovative approaches in both monomer/polymer design and recycling/depolymerization technologies are needed. In addition, delivering tunable material properties for single-monomer-based polymers through their topological variations without changing their chemical composition capitalizes on the many potential benefits of the monomaterial product design.[50] Accordingly, this work designs a bifunctional monomer that can be polymerized by a mixed chain-growth and step-growth polymerization mechanism, leading to an HBPE with tunable molar mass and architecture (e.g., the degree of branching and density of functional groups). Importantly, this HBPE, besides its unique properties and potential applications compared to its linear counterpart, exhibits full chemical circularity through a quantitatively selective cascade depolymerization process, while interestingly, the depolymerization of its linear analogue proceeds through a pretopological transformation to the HBPE, thus also adopting this unique topology-accelerated depolymerization.

RESULTS AND DISCUSSION

Monomer Design for Circular HBPE. To rationally design a monomer toward achieving a HBPE with intrinsic chemical recyclability, we considered the following three critical elements. First, utilizing the ring-opening polymerization (ROP) of lactones, an established method for synthesizing polyesters with well-defined chain structures and controllable molar mass, we chose a hybrid bicyclic lactone (BiL) exhibiting both high and low ceiling temperature lactone moieties as the core structure of our designed monomer, as the BiL was shown previously to produce the corresponding polyester PBiL with intrinsic chemical circularity.[51−53] Second, installation of a pendent hydroxy group on the BiL ring generates bifunctional bicyclic lactone monomer BiL^{OH} (4-hydroxy-6-oxabicyclo[3.2.1]octan-7-one (Scheme 1). We reasoned that bifunctional BiL^{OH} could serve as both an initiator (initiation by the OH group) and a monomer (ROP by the BiL), i.e., an *inimer*. Third, the polymerization of inimer BiL^{OH} could involve a mixed "chain-growth" and "step-growth"-like polymerization mechanism. The "chain-growth" ROP pathway would involve continuous addition of monomer, via either nucleophilic attack of monomer by the propagating hydroxy chain end (route a) or attack of the propagating lactone chain end by the hydroxy group on the monomer (route b), Scheme 1 (blue arrows for a and b). The "step-growth" propagation is proposed to be coupling of the growing chains via nucleophilic attack of the lactone chain end by the hydroxyl chain end (Scheme 1, red arrow). Overall, the combination of the bifunctional inimer structure in BiL^{OH} with the mixed propagation mechanism was hypothesized to generate HBPE, denoted as *hb*-PBiL^{OH}. Note that ring-opening of BiL^{OH} will generate two different OH groups attached to the cyclohexane ring that can be utilized for further polymer chain growth: *para*-OH and *meta*-OH, relative to the ester carbonyl group. As a result, the growing chains can be branched out via both *para*- and *meta*-positions, while the chain ends contain both types of OH groups and some yet-opened lactone rings (Scheme 1, green).

Guided by the above hypotheses, we synthesized BiL^{OH} from 3-cyclohexenecarboxylic acid in an overall yield of ∼70%. Notably, this synthesis of BiL^{OH} is *diastereoselective* as the hybrid atom-bridged bicyclic BiL^{OH} is locked in the *cis*-configuration, whereas the *trans*-configurational diastereomer is *precluded* in its monomeric state. This insight also hints at potentially exclusive selectivity for the desired monomer (BiL^{OH}) recovery over other possible isomer(s) during depolymerization (*vide infra*). Note that although this synthesis is diastereoselective, it is not enantioselective, thereby yielding BiL^{OH} as a pair of enantiomers in a racemic form,

https://doi.org/10.1021/jacs.4c00526
J. Am. Chem. Soc. 2024, 146, 9261−9271

Table 1. Results for ROP of BiL^{OH} Catalyzed by TBD[a]

Run no.	[BiL^{OH}]/[TBD]	Conc. (M)	Time (h)	Conv.[b] (%)	M_n[c] (kg mol^{-1})	$Đ$[c] (M_w/M_n)	DB[d]
1	100/1	10	10 (min)	93	66.0	2.78	0.36
2	100/1	5	15 (min)	92	44.4	2.65	0.33
3	100/1	2.5	24	93	39.5	2.05	0.37
4	100/1	1.25	24	88	21.6	1.84	0.53
5	500/1	5	1	95	43.3	2.67	0.44
6[e]	100/1	10	24	94	104	2.07	0.56
7[f]	500/1	5	24	94	87.5	2.31	0.49
8[g]	100/1	2.5	24	97	17.3	2.28	0.52

[a]Conditions: BiL^{OH} = 0.142 g (1 mmol), DMF, room temperature (RT), except runs 6, 7, and 8 with different sets of conditions. [b]Monomer conversion measured by ^{1}H NMR in DMSO-d_6 of the quenched solution in benzoic acid/DMSO-d_6. [c]Weight-average molar mass (M_w), number-average molar mass (M_n), and dispersity indices ($Đ = M_w/M_n$) determined by size-exclusion chromatography (SEC) at 40 °C in DMF with 10 mM LiBr. [d]Degree of branching (DB) determined by ^{13}C NMR spectroscopy. [e]BiL^{OH} = 1.42 g (10 mmol), DMF, RT. [f]BiL^{OH} = 1.42 g (10 mmol), DMSO-d_6 as the solvent, RT. [g]BiL^{OH} = 0.142 g (1 mmol), DMF, RT, BnOH as initiator, [BiL^{OH}]/[TBD]/[BnOH] = 100:1:1.

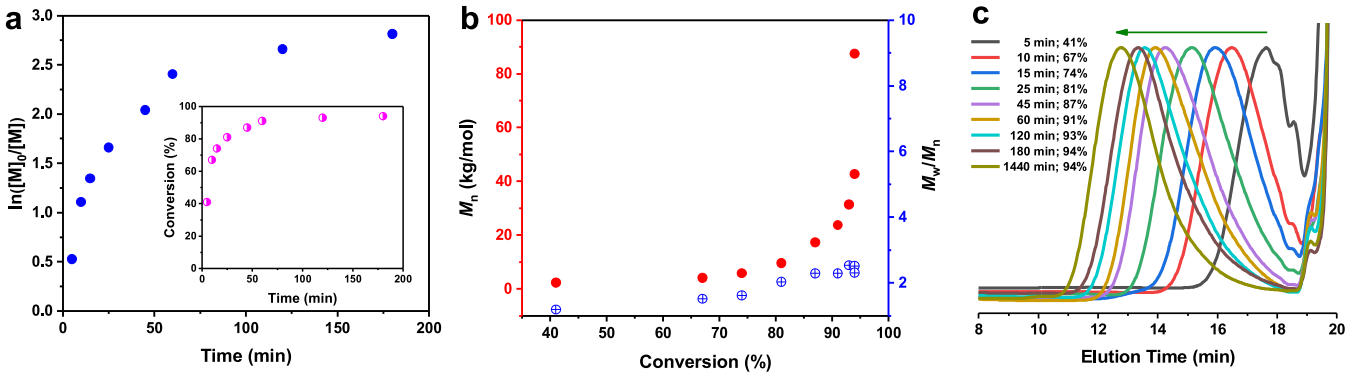

Figure 1. (a) Semilogarithmic kinetic plot of the ROP with [BiL^{OH}]/[TBD] = 500:1 ([BiL^{OH}]$_0$ = 5.0 M, DMSO-d_6, RT). (b) Plots of M_n and $Đ$ values of *hb*-PBiL^{OH} vs BiL^{OH} conversion. (c) Overlays of SEC traces of polymerization aliquots with increasing conversion.

(±)-BiL^{OH}, which is employed for most polymerization studies here. However, the optically pure enantiomer (1*S*, 4*S*, 5*S*)-BiL^{OH} can be readily obtained using the (*S*)-(−)-3-cyclohexenecarboxylic acid precursor and is used for the synthesis of *chiral hb*-PBiL^{OH} for comparative studies (*vide infra*). In addition, as shown by the molecular structure derived from single-crystal X-ray diffraction analysis, the pendant −OH in BiL^{OH} adopts an *exo*-position relative to the plane of the cyclohexane ring (Scheme 1). Hence, BiL^{OH} could function as an effective inimer, which obviates the necessity for an additional initiator, typically required in conventional ROP, and also renders the HBPE structure (*vide supra*).

Evidence for Mixed Mechanism for *hb*-PBiL^{OH} Synthesis. At the outset, organic base TBD (1,5,7-triazabicyclo[4.4.0]dec-5-ene) was employed as the catalyst, as it has been widely recognized as one of the most effective, commercially available organocatalysts for the ROP of lactones.[54,55] Dimethylformamide (DMF) was selected as the solvent, considering the solubility of resulting *hb*-PBiL^{OH}. The polymerization behavior of BiL^{OH} and characteristics of the resulting *hb*-BiL^{OH}, such as number-average molar mass (M_n), dispersity ($Đ = (M_w/M_n)$, and degree of branching (DB), were investigated systematically by varying polymerization conditions (monomer concentration, catalyst loading, etc.). More specifically, when the polymerization was conducted at high initial monomer concentrations (10 and 5 M) (Table 1, runs 1 and 2), the reaction gelled within minutes and achieved high monomer conversions of >90%. While lowering the monomer concentration to 2.5 M (Table 1, run 3), the reaction remained homogeneous throughout the polymerization and reached 93% conversion after 24 h, affording *hb*-BiL^{OH} with an M_n of 39.5 kg mol^{-1} and a dispersity of $Đ$ = 2.05. By further decreasing the monomer concentration to 1.25 M, 88% conversion was achieved in 24 h to give *hb*-BiL^{OH} with a lower M_n of 21.6 kg mol^{-1} and $Đ$ = 1.84 (Table 1, run 4). Lowering the catalyst loading from 1 to 0.2 mol % ([BiL^{OH}]/[TBD] = 500:1) did not affect the M_n and $Đ$ values of the resulting *hb*-PBiL^{OH}, except for a slower polymerization (Table 1, run 5 vs 2; Figures S8 and S9). A gram-scale polymerization conducted at 10 M in DMF was highly exothermic and reached 92% conversion in 2 min, affording a M_n of 37.8 kg mol^{-1} and a dispersity of $Đ$ = 3.09. Extending the polymerization time to 5 min increased the conversion to 94%, and the M_n of the resulting polymer increased significantly to 89.0 kg mol^{-1} with a narrower dispersity ($Đ$ = 2.49). Noteworthy here is that the monomer conversion did not increase noticeably even after 24 h; however, the M_n of the resulting polymer further increased to 103.9 kg mol^{-1} with a narrower dispersity of $Đ$ = 2.07 (Table 1, run 6). Overall, the above results revealed some step-growth polymerization characteristics for the ROP of BiL^{OH}, especially at a later stage of the polymerization.

To obtain further evidence of the late-stage step-growth polymerization behavior, we carried out a kinetic study of BiL^{OH} polymerization with a ratio of [BiL^{OH}]/[TBD] = 500:1 in DMSO-d_6 and an initial concentration of [BiL^{OH}]$_0$ = 5 M (Table 1, run 7). The observed rate constant (k_{obs}), obtained from the slope of the first-order kinetic plot of ln([M]$_0$/[M$_t$]) as a function of time, decreased with time as the monomer was consumed, showing typical chain-growth ROP behavior at the early stage of polymerization (Figure 1a, *vide infra*). The SEC

https://doi.org/10.1021/jacs.4c00526
J. Am. Chem. Soc. 2024, 146, 9261−9271

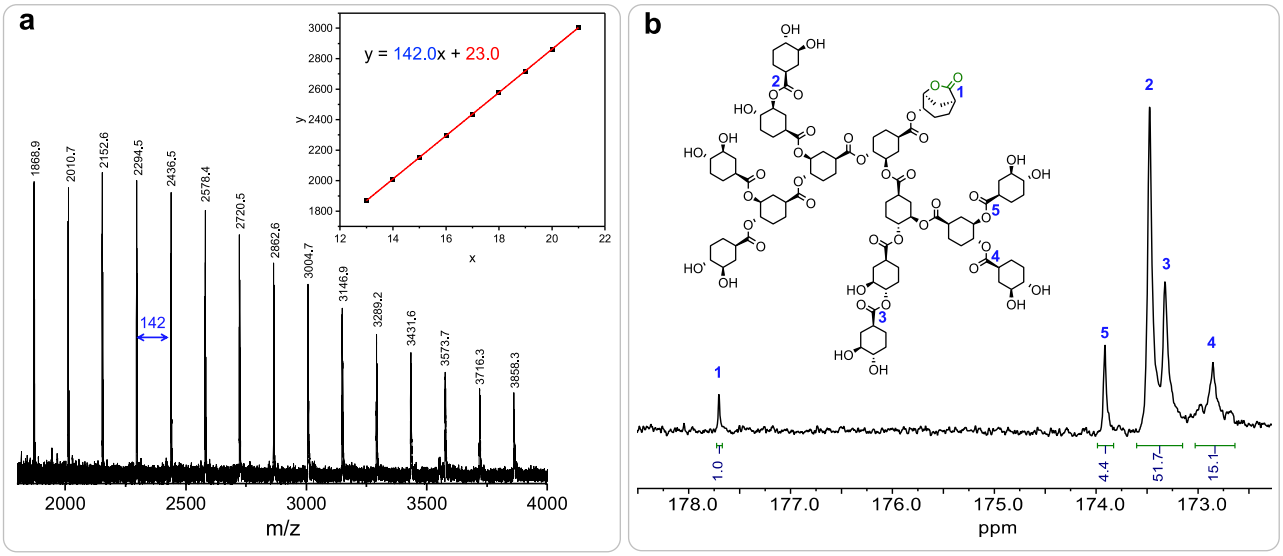

Figure 2. (a) MALDI-TOF MS spectrum of *hb*-PBiL^{OH} produced with [BiL^{OH}]/[La−N] = 500:1 (Table S1, run 2). Inset: plot of m/z values (y) vs the theoretical number of *hb*-PBiL^{OH} repeat units (x). (b) Assignments of carbonyl peaks and DB calculation for *hb*-PBiL^{OH} produced by La−N at RT in DMF.

profiles revealed that the M_n increased with an increase in monomer conversion, as expected, but the M_n increased slowly below 90% conversion and then exponentially when approaching the end of polymerization (Figure 1b), which is consistent with the general step-growth polymerization mechanism at its late stage. This conclusion was further confirmed by the polymerization result that addition of an additional initiator, benzyl alcohol (BnOH), yielded *hb*-PBiL^{OH} with the lowest M_n (Table 1, run 8), compared to the *hb*-PBiL^{OH} samples obtained under the similar polymerization condition but without the additional initiator (vs Table 1, run 3). More specifically, the BnOH-initiated hyperbranched oligomer would not proceed with the coupling of two low molar mass *hb*-PBiL^{OH} chains via the "step-growth" like mechanism (Scheme 1) because BnOH functions as the chain-end-capping reagent. Taken together, it appears that the polymerization of BiL^{OH} follows a mixed-chain growth and step-growth mechanism. The chain-growth ROP process encompasses two monomer-addition scenarios: the chain end −OH of the formed oligomer ring opens monomer BiL^{OH} (Scheme 1, route a) and the pendent −OH group of BiL^{OH} ring-opens the chain-end lactone of the growing oligomer (Scheme 1, route b). This process is characteristic of the chain-growth ROP mechanism, as the monomer is continuously added to the growing chain. When most or all monomer is consumed at later stages of polymerization, the step-growth process takes over via coupling of oligomeric chains, resulting in exponential growth of the polymer molar mass (Scheme 1, red arrow).

Structure Elucidation of *hb*-PBiL^{OH}. To facilitate spectral assignments of complex NMR spectra of *hb*-PBiL^{OH} (Figures S10−S12), which is produced as a mixture of stereoisomers from racemic (±)-BiL^{OH}, we set out to synthesize chiral (1*S*, 4*S*, 5*S*)-*hb*-PBiL^{OH} from chiral inimer (1*S*, 4*S*, 5*S*)-BiL^{OH} prepared from the chiral precursor (*S*)-(−)-3-cyclohexene-carboxylic acid (see the Supporting Information for details). Both commercially available organic catalyst TBD (Table S1, run 1) and metal-based catalyst La[N(SiMe$_3$)$_2$]$_3$ (La−N), also known for its high effectiveness in catalyzing the coordination−insertion ROP of cyclic esters,[13] were shown to be efficient in catalyzing the polymerization of (1*S*, 4*S*, 5*S*)-BiL^{OH}. A notable difference between the polymerizations of chiral and racemic BiL^{OH} is that semicrystalline (1*S*, 4*S*, 5*S*)-*hb*-PBiL^{OH} precipitated out of the concentrated solution (5.0 M), thus preventing further chain coupling to higher molar mass HBPE (M_n = 7.1 kg mol^{-1}, Table S1, run 2). This issue was resolved by lowering the $[M]_0$ to 2.5 M and increasing the La−N loading from 0.2 to 1 mol %, which prevented the premature precipitation and thus achieved a much higher molar mass (1*S*, 4*S*, 5*S*)-*hb*-PBiL^{OH} (M_n = 40.4 kg mol^{-1}, $Đ$ = 2.18, Table S1, run 3).

As expected, the ^{13}C NMR spectrum of (1*S*, 4*S*, 5*S*)-*hb*-PBiL^{OH} is considerably simpler than that of *hb*-BiL^{OH} (Figure S13). In addition, (1*S*, 4*S*, 5*S*)-*hb*-PBiL^{OH} is semicrystalline, exhibiting a melting-transition temperature (T_m) of 196 °C on the first DSC (differential scanning calorimetry) heating scan (Figure S16), whereas *hb*-PBiL^{OH} is amorphous, displaying only a glass-transition temperature (T_g) of 191 °C (Figure S14). The semicrystalline nature of (1*S*, 4*S*, 5*S*)-*hb*-PBiL^{OH} was further confirmed by its wide-angle X-ray scattering profile, which displayed sharp diffraction peaks at 2θ values of 18.2°, relative to an amorphous reference *hb*-PBiL^{OH} sample produced from BiL^{OH} by TBD (Figure S17). Furthermore, (1*S*, 4*S*, 5*S*)-*hb*-PBiL^{OH} is optically active, displaying a specific rotation of $[\alpha]^{24}_{589}$ = +82.0 deg dm^{-1} g^{-1} cm^3 in DMF. This value is three times that of chiral monomer (1*S*, 4*S*, 5*S*)-BiL^{OH}, highlighting the chiral amplification by the hyperbranched topology of (1*S*, 4*S*, 5*S*)-*hb*-PBiL^{OH}.

The chain structure of the resulting HBPE was further characterized by matrix-assisted laser desorption/ionization−time-of-flight mass spectrometry (MALDI-TOF MS). The MALDI-TOF mass spectrum of a low-molecular-weight sample of *hb*-PBiL^{OH} showed an identical spacing between adjacent peaks, corresponding to the exact molar mass of the repeat unit (m/z = 142.0), as shown by the slope (142.0) of the linear plot of m/z values (y) vs the number of *hb*-PBiL^{OH} repeat units (x) (Figure 2a). The intercept of the plot, 23.0, represents the mass of Na$^+$, indicating that the molar mass was

https://doi.org/10.1021/jacs.4c00526
J. Am. Chem. Soc. 2024, 146, 9261−9271

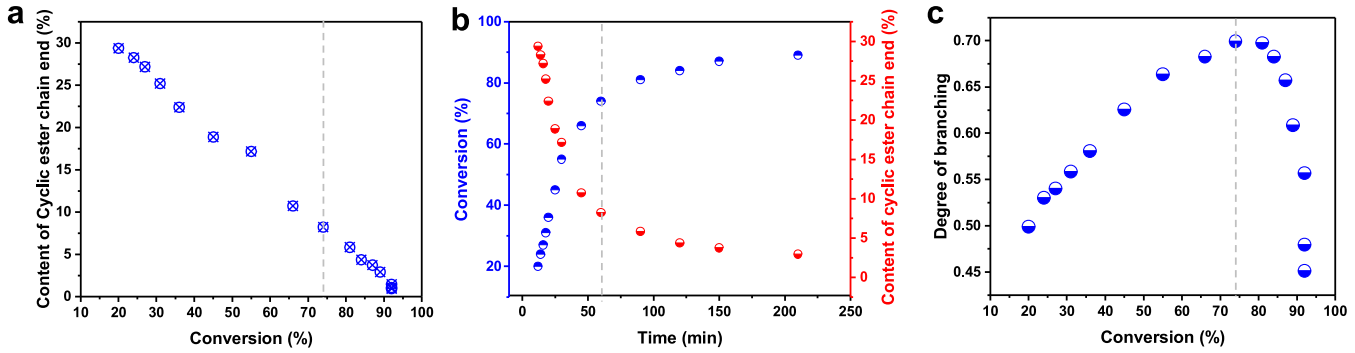

Figure 3. (a) Content of lactone chain end values as a function of BiL^{OH} conversion. (b) Conversion and content of lactone chain end values as a function of polymerization time. (c) DB values as a function of BiL^{OH} conversion.

an integral multiple of the monomer unit, consistent with the hyperbranched structure. This structure created by the free −OH group in *hb*-$PBiL^{OH}$ was further confirmed by ^{13}C NMR. Notably, the carbonyl group of the unopened lactone can be observed at 177.7 ppm (peak 1, Figure 2b), which disappeared in the high-molecular-weight sample (Figure S18). The DB, an essential parameter for hyperbranched polymers, was calculated according to the equation DB = $2D/(2D + L)$,[56,57] where D represents the number of dendritic units and L signifies the number of linear units, the values of which can be obtained from the integration of the split carbonyl peak in ^{13}C NMR spectra.

Lastly, we performed an in-depth analysis of cyclic ester (lactone) chain end and DB variations as a function of monomer conversation and polymerization time by monitoring a polymerization performed in DMSO-d_6 at $[M]_0$ = 2.5 M with $[BiL^{OH}]/[TBD]$ = 500:1 (Table S2). As discussed above for the polymerization in 5.0 M, the M_n here also displayed a gradual, small increase up to 90% conversion, followed by an exponential rise toward the completion of polymerization (Figure S19a). However, by focusing on the early stage of the polymerization, the chain-growth polymerization behavior was evident by the observed linearity of the first-order kinetic plot (Figure S19c) and linear increase in M_n with monomer conversion while the $Đ$ value remained nearly constant (up to 36% conversion, Figure S19b). Importantly, the *in situ* study here tracked the evolution of the microstructure of the resulting HBPE using ^{13}C NMR at specific time intervals (Figure S20). In particular, the proportion of the lactone chain ends decreased linearly as a function of the increasing monomer conversion (Figure 3a). Noteworthy here is that the ring-opening of the chain-end lactone by the pendent −OH group of inimer BiL^{OH} (Scheme 1, route b) or the ring-opening of BiL^{OH} by the chain-end OH group (Scheme 1, route a) leads to an increase in the total number of ester linkages without altering the total number of chain-end lactones (but its percentage relative to the ester linkages decreases). In contrast, in the step-growth process, each coupling of two growing HBPE chains results in the net consumption of one chain-end lactone. As a result, both the chain-growth and step-growth processes contribute to the decrease in the percentage content of chain-end lactones (Figures 3a). The plots of monomer conversion and chain-end lactone content values as a function of polymerization time suggest that as the monomer conversion increases, the chain-end lactone content decreases correspondingly (Figures 3b and S21). Notably, even upon reaching an equilibrium monomer conversion, the content of the chain-end lactones persists in decline, attributable to the step-growth process (*vide supra*). Throughout the polymerization, the DB experienced an initial increase in tandem with increasing the conversion before encountering a steep decline. The apex of the DB was achieved at 0.7 at approximately 74% conversion (with the specific value falling within the 74−81% range) within 1 h. At this stage, the polymer molar mass is relatively low (∼3−4 kDa). Following this point, the DB decreases as the molar mass experiences an exponential increase (Figure 3c). The decrease in the DB can be attributed to the rise in steric hindrance at the chain end that occurs as the HBPE grows. This increase in steric hindrance renders it difficult to initiate further monomer addition at both (*para*- and *meta*-) OH chain ends, ultimately resulting in the formation of linear units rather than further branching at the late stage of polymerization.

Depolymerization Ability and Selectivity of *hb*-$PBiL^{OH}$. To assess the depolymerizability of the resulting HBPE, the thermodynamics of the BiL^{OH} polymerization was probed using the polymerization with $[M]/[TBD]$ = 100:1 at $[M]_0$ = 0.5 M in DMSO-d_6 via the variable-temperature NMR method. The equilibrium monomer concentration, $[M]_{eq}$, obtained by plotting $[M]_t$ as a function of time until $[M]$ became constant, was used for the van't Hoff plot of $\ln[M]_{eq}$ vs $1/T$, from which thermodynamic parameters were calculated to be ΔH_p^o = −28.2 kJ·mol^{-1} and ΔS_p^o = −76.9 J·mol^{-1}·K^{-1} (Figures S22 and S23). The ceiling temperature (T_c) was calculated to be 366 K (93 °C) when extrapolated to $[M]_{eq}$ = 1.0 M, based on the equation $T_c = \Delta H_p^o/\{\Delta S_p^o + R \ln[M]_{eq}\}$. These parameters indicate a good balance for both the polymerizability of BiL^{OH} and the depolymerizability of *hb*-$PBiL^{OH}$, the direction of which can be manipulated by adjusting the reaction temperature and concentration (i.e., high temperature and low concentration favor depolymerization, *vice versa*).

It is worth noting here that *hb*-$PBiL^{OH}$ contains two types of hydroxy groups on the cyclohexane ring (*para*- or *meta*- relative to the ester bond) at the polymer chain end. Hence, there could be two potentially competing depolymerization modes, leading to two possible depolymerization monomer products, the original building-block monomer BiL^{OH} and its isomer [2,2,2]BiL^{OH} containing two 6-membered lactone rings (Scheme 2, red). However, the depolymerization run catalyzed with 1.0 mol % La−N and carried out in DMSO-d_6 at 120 °C for 3 h afforded only one monomer product, BiL^{OH} (Figure 4). TBD was also shown to be effective for the selective depolymerization of *hb*-$PBiL^{OH}$ to BiL^{OH} under the same

https://doi.org/10.1021/jacs.4c00526
J. Am. Chem. Soc. 2024, 146, 9261−9271

Scheme 2. Selectivity in Depolymerization of *hb*-PBiL^{OH}

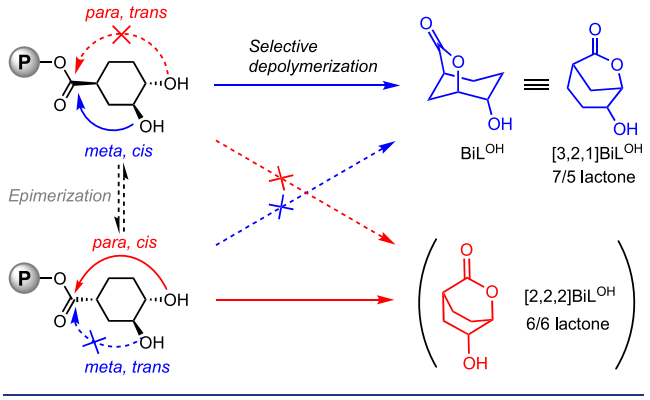

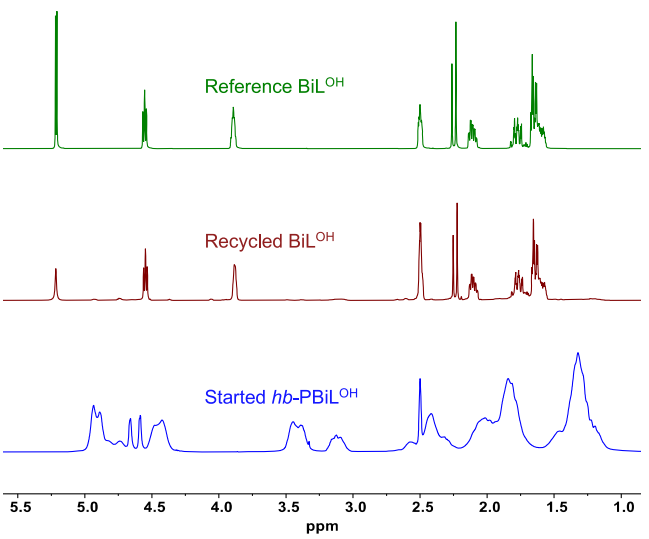

Figure 4. Overlays of ^{1}H NMR spectra (23 °C, DMSO-d_6) of *hb*-PBiL^{OH} (Table 1, run 5, bottom), recovered crude monomer product BiL^{OH} after depolymerization (DMSO, 1.0 mol % La–N, 120 °C, 3 h, middle), and starting BiL^{OH} for comparison (upper).

depolymerization condition. These results demonstrated the exclusive depolymerization selectivity of *hb*-PBiL^{OH} for reforming its monomer BiL^{OH}. We reasoned that this exclusive selectivity is controlled by the defined relative stereochemistry between the two hydroxy groups and the ester carbonyl: *trans* for *para*-OH and *cis* for *meta*-OH (Scheme 2). It would seem apparent that nucleophilic attack of the ester carbonyl by *meta*-OH is an energetically favored process, while the hypothesized attack by *para*-OH is forbidden, explaining the exclusive selectivity. Conversely, to form the isomer [2,2,2]BiL^{OH}, epimerization at the α-carbon of the carbonyl group must occur first to configurationally arrange the ester group to be *cis* to the *para*-OH (Scheme 2). The results that the same exclusive selectivity was observed for both coordination catalyst La–N and basic catalyst TBD imply that, under these conditions, epimerization is not operative.

To ascertain the underlying mechanism that is responsible for precluding [2,2,2]BiL^{OH} formation, density functional theory (DFT) calculations at the M062X/Def2-TZVP level with inclusion of the D3 dispersion corrections were carried out.[58−60] These computations were executed on two potential depolymerization pathways, catalyzed by the TBD, to determine if energy disparities could clarify the exclusive formation of BiL^{OH}. The depolymerization model for BiL^{OH} formation, depicted in Figure S24, draws inspiration from the computational research of Simón and Goodman[61] and Chuma et al.[62] We selected a simple, unbranched dimer compound with two vacant terminal hydroxyl groups as a representative model for the chain-end of *hb*-PBiL^{OH}. Figure S25 compares the enthalpies for both the BiL^{OH} and [2,2,2]BiL^{OH} pathways when both *meta*- and *para*-OH groups are allowed to be *cis* to the carbonyl. In the early stages, the formation of a prereaction complex is marginally more energetically favorable for BiL^{OH} due to lower ring strain in its chair geometry, compared to the boat conformation in the [2,2,2]BiL^{OH} pathway. Beyond this stage, the enthalpy barriers through the first transition states are virtually identical, suggesting that any strain-induced enthalpy variations are fully accounted for in the prereaction complex. Subsequent steps show convergence in the formation of the first intermediate species with minimal energetic differences upon reorientation of the TBD catalyst. The second energy barrier is notably lower for [2,2,2]BiL^{OH}, implying that it is kinetically more favorable. While definitive conclusions are elusive, we hypothesize that variations in hydrogen bonding structures may contribute significantly to the differences in barrier heights. This is corroborated by a greater enthalpy loss in the final monomer-release step of the [2,2,2]BiL^{OH} pathway, attributed solely to the loss of noncovalent interactions among the complex's three fragments. Given that only BiL^{OH} is observed experimentally, despite [2,2,2]BiL^{OH} being kinetically more favorable (when the *para*-OH is allowed to be *cis* to the carbonyl), we concluded that epimerization is suppressed in this system. This is likely due to a combination of insufficient basicity of the catalyst and the high concentration of hydroxyl groups in the polymerization system, which inhibits epimerization at the α-carbon of the carbonyl group.

Topology-Accelerated Cascade Depolymerization. To investigate the effects of topology on the depolymerization rate and selectivity, a linear analogue, *l*-PBiL^{OH}, was synthesized, which was achieved using a OH-protection/deprotection strategy (Figures S26–S30). Specifically, the *tert*-butoxycarbonyl group (Boc-) protected monomer BiL^{OBoc} was prepared from BiL^{OH} (Figures S3–S5). Subsequently, its polymerization was carried out in a [BiL^{OBoc}]/[TBD]/[BnOH] = 300:1:1 at RT, yielding a linear precursor, *l*-PBiL^{OBoc}, with M_n = 55.5 kg mol^{-1} and $Đ$ = 1.49 (Figures S26–S28). Deprotection of the Boc-group with trifluoracetic acid (TFA) afforded *l*-PBiL^{OH} with M_n = 37.5 kg mol^{-1} and $Đ$ = 1.45) (Figures S29 and S30). The constant polymer dispersity before and after TFA treatment suggests that no noticeable transesterification or chain scission occurred during the deprotection procedure. Further evidence comparing the ^{1}H NMR spectra of the obtained *l*-PBiL^{OH} with that of *hb*-PBiL^{OH} supported this conclusion; otherwise, the branching signal would appear in the ^{1}H NMR of *l*-PBiL^{OH} (Figure S29). The thermal stability of *l*-PBiL^{OH} as measured by its $T_{d5\%}$ (decomposition temperature at 5% mass loss) of 277 °C and T_{max} (maximum rate decomposition temperature) of 297 °C (Figure S31) is noticeably lower than that of *hb*-PBiL^{OH} ($T_{d5\%}$ = 295 °C and T_{max} = 342 °C, Figure S15). On the other hand, both *hb*-PBiL^{OH} and *l*-PBiL^{OH} exhibited similarly high T_g values at 191 and 197 °C, respectively (Figures S14 and S32), attributable to the strong hydrogen bonds formed between inter and intramolecular interactions.[63]

The differences in flow and shearing profiles between *hb*-PBiL^{OH} and *l*-PBiL^{OH} were investigated using rheological

https://doi.org/10.1021/jacs.4c00526
J. Am. Chem. Soc. 2024, 146, 9261−9271

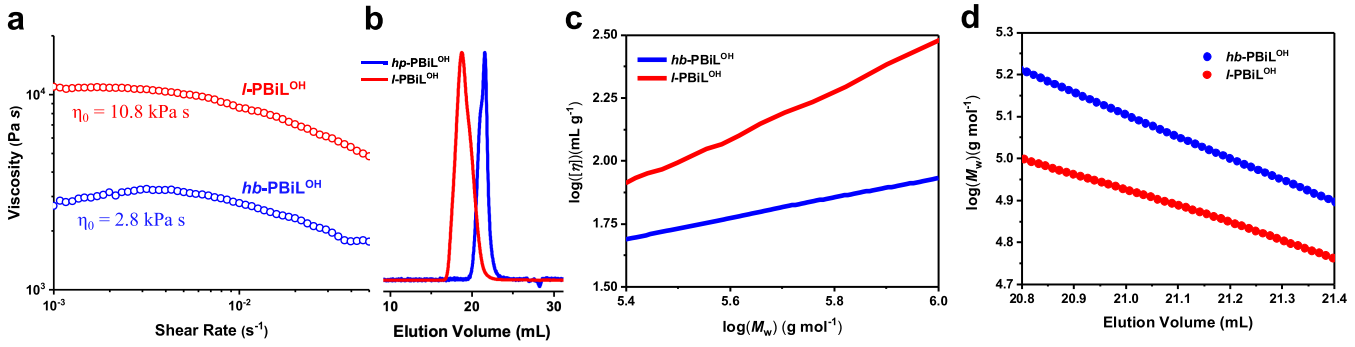

Figure 5. (a) Rheological bulk viscosity profiles (175 °C) of *l*-PBiL^{OH} (M_n = 37.5 kg mol^{-1}, $Đ$ = 1.45) and *hb*-PBiL^{OH} (M_n = 43.3 kg mol^{-1}, $Đ$ = 2.67). (b) SEC profiles of *l*-PBiL^{OH} and *hb*-PBiL^{OH} obtained from an 18-angle light scattering detector. (c) Double logarithm (base 10) plots of intrinsic viscosity [η] as a function of absolute M_w of *l*-PBiL^{OH} and *hb*-PBiL^{OH} (Mark−Houwink−Sakurada plot), obtained by a Malvern Visotek 305 triple detector. (d) Logarithm (base 10) plots of M_w as a function of the elution volume of *l*-PBiL^{OH} and *hb*-PBiL^{OH}, obtained by a Malvern Visotek 305 triple detector. All red lines or curves for *l*-PBiL^{OH} and blue ones for *hb*-PBiL^{OH}.

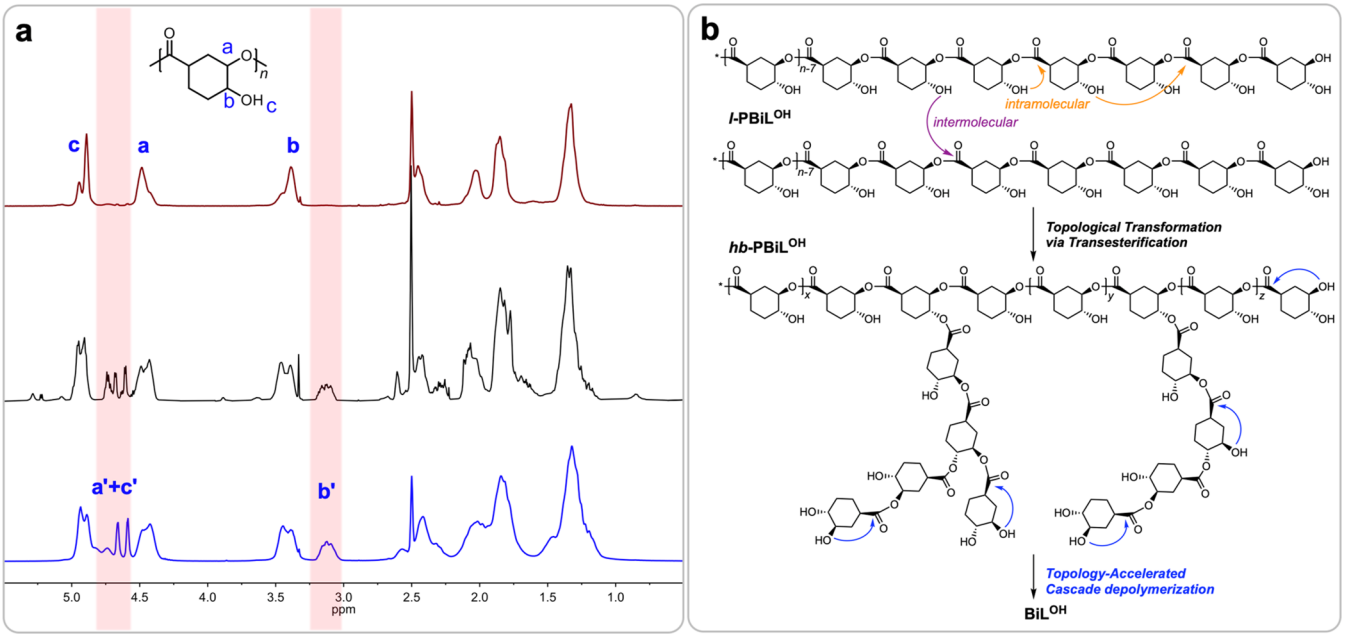

Figure 6. (a) Overlays of ^{1}H NMR spectra (23 °C, DMSO-d_6) of *l*-PBiL^{OH} (M_n = 37.5 kg mol^{-1}, $Đ$ = 1.45, upper), *l*-PBiL^{OH} depolymerization mixture after 0.5 h (120 °C, 0.2% La−N, middle), and *hb*-PBiL^{OH} (M_n = 43.3 kg mol^{-1}, $Đ$ = 2.67, bottom) for comparison (highlighted peaks labeled with ' show signature peaks for *hb*-PBiL^{OH}, which differentiate the two topologies). (b) Schematic representation of the *l*-PBiL^{OH} depolymerization process involving topological transformation via transesterification from its linear structure to the hyperbranched topology that in turn accelerates the chain-end unzipping process.

viscosity and angular frequency sweeps in the bulk. Under similar shearing conditions (175 °C, 10 rad s^{-1}), the viscosity (η_0 = 2.8 kPa s) of the hyperbranched network in *hb*-PBiL^{OH}, unencumbered by chain entanglement, was noticeably lower compared to that of the linear counterpart (η_0 = 10.8 kPa s) in *l*-PBiL^{OH} (Figure 5a). Frequency sweeps at a higher temperature (190 °C) revealed that *hb*-PBiL^{OH} lacks a G' (shear storage modulus) − G'' (shear loss modulus) crossing point (relaxation time) under the same processing conditions (Figure S35), while *l*-PBiL^{OH} does transition to the "rubbery plateau" at a shear rate of 8.7 rad s^{-1}, corresponding to a fast relaxation time of 0.12 s, likely supported by hydrogen-bonding elasticity (Figures S36). It is hypothesized that the HBPE's network architecture does not experience chain relaxation, as chains cannot pack or separate independently in response to stress or recovery in the traditional linear polymer fashion.

The solution properties of *hb*-PBiL^{OH} and *l*-PBiL^{OH} were compared using SEC (Figure 5b) with triple detection (light-scattering detector, refractometer, and a viscometer). A double-logarithm (Mark−Houwink−Sakurada) plot of intrinsic viscosity [η] in DMF as a function of absolute M_w in the overlapped molar mass regime (Figure 5c) revealed a lower intrinsic viscosity for *hb*-PBiL^{OH} due to its smaller hydrodynamic volume, compared to *l*-PBiL^{OH}. The logarithmic plots of M_w versus elution volume further substantiated that *hb*-PBiL^{OH} has a hydrodynamic volume smaller than that of *l*-PBiL^{OH} (Figure 5d).

Taking advantage of the high OH content of PBiL^{OH}, postfunctionalization was performed using *tert*-butyldimethylsilyl chloride, yielding the corresponding *l*-PBiL^{OSiR3} and *hb*-PBiL^{OSiR3} (Figures S37−S38, and S41−S42). Both products

https://doi.org/10.1021/jacs.4c00526
J. Am. Chem. Soc. 2024, 146, 9261−9271

exhibit high thermal stability, with $T_{d,5\%}$ values of 328 °C for *l*-PBiL^{OSiR3} and 338 °C for *hb*-PBiL^{OSiR3}, respectively (Figures S39 and S43). Notably, after the consumption of the −OH groups, T_g decreased to 168 °C for *l*-PBiL^{OSiR3} and 145 °C for *hb*-PBiL^{OSiR3}, respectively (Figures S40 and S44), underlining the significant contribution of hydrogen bonds to the high T_g values of *l*-PBiL^{OH} and *hb*-PBiL^{OH}. The SEC profiles of *l*-PBiL^{OSiR3} and *hb*-PBiL^{OSiR3} (Figures S45−S47) mirrored the trends observed with *l*-PBiL^{OH} and *hb*-PBiL^{OH}, further confirming the impact of topology on solution behavior. Additionally, the modification of the monomer and *hb*-PBiL^{OH} emphasizes the potential for postfunctionalization in this system, demonstrating its adaptability for a range of possible applications.

The depolymerization behavior of *l*-PBiL^{OH} (Figure 6a) is the most intriguing. We initially assumed that the depolymerization of *l*-PBiL^{OH} would be significantly slower than that of *hb*-PBiL^{OH}, as the *meta*-hydroxy group (relative to the ester carbonyl) that triggers the chain-end unzipping process (Scheme 2) is present only at the chain end of the linear polymer (Figure 6b). In comparison, *hb*-PBiL^{OH} possesses multiple *meta*-hydroxy groups (Figure 2c), allowing *hb*-PBiL^{OH} to initiate the fast unzipping depolymerization process from multiple chain ends simultaneously, the phenomenon of which we termed topology-accelerated cascade depolymerization. Surprisingly, *l*-PBiL^{OH} also underwent rapid depolymerization and completely transformed into BiL^{OH} in just 3 h (Figure S48) under the same depolymerization conditions employed for *hb*-PBiL^{OH} (Figure 4). To better monitor the depolymerization process of *l*-PBiL^{OH}, a lower catalyst loading was used to slow the reaction for observing possible intermediate(s). Specifically, the depolymerization of *l*-PBiL^{OH} in DMSO-d_6 at 120 °C with only 0.2% La−N catalyst was monitored *in situ* by ^{1}H NMR. Intriguingly, the results revealed that transesterification occurred first during the depolymerization of *l*-PBiL^{OH}, which generated the same branched structure as that of *hb*-PBiL^{OH} (Figure S49), thus in turn accelerating the depolymerization process (Figure 6). Noteworthy also is the fact that the results of the kinetic study on the depolymerization of linear PBiL^{OH} showed that almost no monomer was generated within the initial 0.5 h; however, during the same time period clear transformation from the linear to hyperbranched topology had already occurred extensively (Figure S49), further supporting the proposed topological transformation prior to the possible chain-unzipping directly from the *l*-PBiL^{OH} and topology-accelerated depolymerization mechanism.

Exploring Potential Applications for *hb*-PBiL^{OH}. Considering its high hydroxy content as well as its tunable molar mass and architecture, we explored potential applications for *hb*-PBiL^{OH} as an adhesive, a rheology modifier, and an additive for property reinforcement. Based on our initial screening, the most promising of these applications was identified as a reinforcing additive for rigid poly(vinyl chloride) (PVC). Although these materials do not plasticize the PVC (*vide infra*), they do impart flexibility which may enable them to displace phthalate-based plasticizers or other molecules depending on the application. Initially, a THF solution containing 9 wt % PVC and 1 wt % *hb*-PBiL^{OH} was studied as a function of *hb*-PBiL^{OH} molar mass from M_n = 13 kDa to 100 kDa (Figure 7a). Although *hp*-PBiL^{OH} is not readily soluble in THF, it becomes soluble in a solution of THF and PVC. Relative to the starting PVC solution, the presence of *hb*-PBiL^{OH} increases the solution viscosity from 1.13 mPa to 1.31 mPa at 13 kDa, indicating a positive interaction between *hb*-PBiL^{OH} and PVC. As the molar mass of *hb*-PBiL^{OH} is increased, the viscosity increased further (2.14 mPa at 100 kDa), supporting the beneficial interaction between *hb*-PBiL^{OH} and PVC. Different architectures were also tested at M_n = 38 kDa; while both *hp*-PBiL^{OH} and *l*-PBiL^{OH} increased the solution viscosity (Figure 7b) with PVC, the *hb*-PBiL^{OH} increased the solution viscosity about 35% more than the *l*-PBiL^{OH} (1.77 mPa vs 1.31 mPa). This result aligns with the solution property results and further supports that the architecture of *hb*-PBiL^{OH} enables a synergistic interaction with multiple branched chains. Following the solution studies to demonstrate compatibility between PVC and *hb*-PBiL^{OH}, films of 50 mol % *hb*-PBiL^{OH} and 50 mol % PVC were prepared by dissolution in THF and subsequent casting. Scanning electron microscopy (SEM) of the resultant films revealed no phase separation between the polymers (Figure 7d versus Figure S51), further supporting the above results. When the 50:50 PVC:*hb*-PBiL^{OH} films were subject to dynamic mechanical analysis (DMA), single phase behavior is also observed (Figure 7c), as evident by one tan δ transition, and the polymer showed an increase in glass transition (61 to 71 °C), also indicating favorable interactions. Additionally, there is softening in the blend material, as shown by the storage modulus; for example, at 35 °C the storage modulus of the blend is 54 Pa, relative to 757 Pa for PVC.

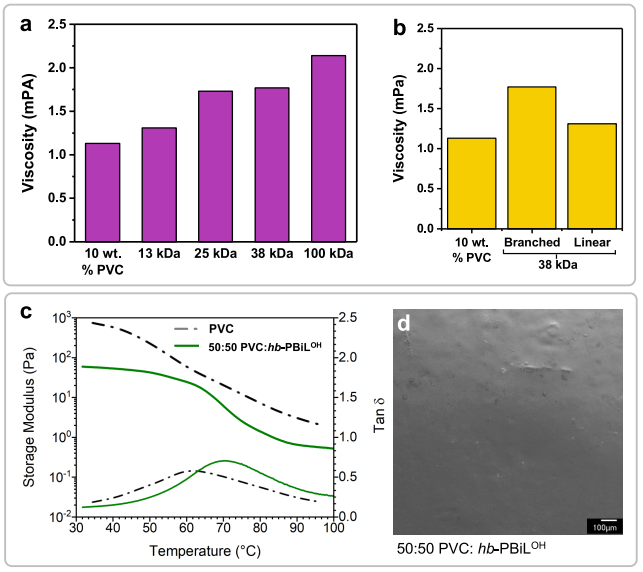

Figure 7. Reinforcement effects of PVC with HBPE. (a). Solution viscosity of 9 wt % PVC and 1 wt % *hb*-PBiL^{OH} in THF as a function of the HBPE molar mass. (b) Solution viscosity for the same system with linear and branched architectures. (c) DMA curves of PVC and 50:50 PVC:*hb*-PBiL^{OH} blend showing only one broad tan δ for the blend, indicating a single-phase material and an elevated glass transition temperature alongside a lower storage modulus. (d) SEM imaging of the 50:50 PVC:*hb*-PBiL^{OH} blend demonstrates no visible phase separation.

Both the synergistic mixing of *hb*-PBiL^{OH} with PVC and the softening of the blend material enable *hb*-PBiL^{OH} to improve the end of life and performance properties of the rigid PVC, due to its ester nature and softening potential, both of which are desirable for PVC.[64] Additionally, as *hb*-PBiL^{OH} is compatible with PVC, it has the potential to find use in

https://doi.org/10.1021/jacs.4c00526
J. Am. Chem. Soc. 2024, 146, 9261−9271

applications where tunable performance is needed. This could include membranes[64,65] for various separations or treatments in which flexibility and chemical combability are required. Interestingly, the results of *hb*-PBiL^{OH} as a reinforcement for PVC represent performance akin to the PVC blend with lignin.[66,67] This indicates that *hb*-PBiL^{OH} could be used as a "synthetic lignin analogue". Note that the example of *hb*-PBiL^{OH} shown here as a compatible and synergistic reinforcement for PVC is not a demonstration of the monomaterial product design—which is based on the premise that both *l*-PBiL^{OH} and *hb*-PBiL^{OH} have the same chemical composition (obtained from the same monomer BiL^{OH}) and can be depolymerized back to the same, single monomer but exhibit distinctly different material properties.

CONCLUSIONS

In summary, here we present a chemically circular HBPE derived from a mixed chain-growth and step-growth polymerization of OH-containing, atom-bridged bicyclic lactone BiL^{OH} that serves as both initiator and monomer (i.e., inimer). Despite its architectural complexity, the resulting HBPE, *hb*-PBiL^{OH}, exhibits exclusive depolymerization selectivity to reform its monomer BiL^{OH}, attributable to its unique cascade polymerization mechanism via chain-end unzipping triggered by the hydroxy groups located at the "*meta*" position of the six-membered ring. For comparative studies of morphology effects on physical properties and material performance, linear analogue *l*-PBiL^{OH} was also synthesized from the same monomer BiL^{OH} by a protection/deprotection strategy. Extensive characterizations of solution, solid-state (thermal and mechanical), and melt (flow and shearing) properties revealed strong topological effects on material properties. Considering the high hydroxy content and tunable architecture of *hb*-PBiL^{OH}, we explored its potential application as a compatible and synergistic reinforcement for PVC. More intriguingly, depolymerization of *l*-PBiL^{OH} proceeds, unexpectedly, through a topological transformation via transesterification to the HBPE architecture first, followed by the faster cascade depolymerization pathway characteristic of *hb*-PBiL^{OH}. Overall, the results reported herein underscore the potential for designing CPs that can go far beyond the typical linear polymers to architecturally more complex structures such as the HBPE presented herein, thus significantly expanding the realm of CPs. Furthermore, the ability to substantially modulate the properties of polymers and also accelerate depolymerization via topological manipulation, without changing monomer composition, bolsters the emerging more sustainable monomaterial product design based on CPs.

ASSOCIATED CONTENT

Supporting Information

The Supporting Information is available free of charge at https://pubs.acs.org/doi/10.1021/jacs.4c00526.

Complete experimental and DFT details, additional figures and tables, and Cartesian coordinates (PDF)

Accession Codes

CCDC 2293755 contains the supplementary crystallographic data for this paper. These data can be obtained free of charge via www.ccdc.cam.ac.uk/data_request/cif, or by emailing data_request@ccdc.cam.ac.uk, or by contacting The Cambridge Crystallographic Data Centre, 12 Union Road, Cambridge CB2 1EZ, UK; fax: +44 1223 336033.

AUTHOR INFORMATION

Corresponding Authors

Linda J. Broadbelt − *Department of Chemical and Biological Engineering, McCormick School of Engineering and Applied Science, Northwestern University, Evanston, Illinois 60208, United States;* orcid.org/0000-0003-4253-592X; Email: broadbelt@northwestern.edu

Eugene Y.-X. Chen − *Department of Chemistry, Colorado State University, Fort Collins, Colorado 80523-1872, United States;* orcid.org/0000-0001-7512-3484; Email: eugene.chen@colostate.edu

Authors

Changxia Shi − *Department of Chemistry, Colorado State University, Fort Collins, Colorado 80523-1872, United States*

Nicholas A. Rorrer − *Renewable Resources and Enabling Sciences Center, National Renewable Energy Laboratory, Golden, Colorado 80401, United States; BOTTLE Consortium, Golden, Colorado 80401, United States;* orcid.org/0000-0001-9134-5853

Alexander L. Shaw − *Department of Chemical and Biological Engineering, McCormick School of Engineering and Applied Science, Northwestern University, Evanston, Illinois 60208, United States*

Ryan W. Clarke − *Renewable Resources and Enabling Sciences Center, National Renewable Energy Laboratory, Golden, Colorado 80401, United States; BOTTLE Consortium, Golden, Colorado 80401, United States*

Bonnie L. Buss − *Renewable Resources and Enabling Sciences Center, National Renewable Energy Laboratory, Golden, Colorado 80401, United States; BOTTLE Consortium, Golden, Colorado 80401, United States*

Gregg T. Beckham − *Renewable Resources and Enabling Sciences Center, National Renewable Energy Laboratory, Golden, Colorado 80401, United States; BOTTLE Consortium, Golden, Colorado 80401, United States;* orcid.org/0000-0002-3480-212X

Complete contact information is available at: https://pubs.acs.org/10.1021/jacs.4c00526

Notes

The authors declare no competing financial interest.

ACKNOWLEDGMENTS

We gratefully acknowledge support by the U.S. Department of Energy, Office of Energy Efficiency and Renewable Energy, Advanced Materials and Manufacturing Technologies Office (AMMTO) and Bioenergy Technologies Office (BETO). This work was performed as part of the Bio-Optimized Technologies to keep Thermoplastics out of Landfills and the Environment (BOTTLE) Consortium and was supported by AMMTO and BETO under Contract DE-AC36-08GO28308 with the National Renewable Energy Laboratory (NREL), operated by Alliance for Sustainable Energy, LLC. The BOTTLE Consortium includes members from Northwestern University and Colorado State University.

REFERENCES

(1) Geyer, R.; Jambeck, J. R.; Law, K. L. Production, use, and fate of all plastics ever made. *Sci. Adv.* **2017**, *3*, e1700782.

(2) Ellen MacArthur Foundation. The New Plastics Economy: Rethinking the future of plastics & catalysing action. https://

ellenmacarthurfoundation.org/the-new-plastics-economy-rethinking-the-future-of-plastics-and-catalysing, 2017 (accessed 2024-01-01).
(3) Borrelle, S. B.; Ringma, J.; Law, K. L.; Monnahan, C. C.; Lebreton, L.; McGivern, A.; Murphy, E.; Jambeck, J.; Leonard, G. H.; Hilleary, M. A.; Eriksen, M.; Possingham, H. P.; De Frond, H.; Gerber, L. R.; Polidoro, B.; Tahir, A.; Bernard, M.; Mallos, N.; Barnes, M.; Rochman, C. M. Predicted growth in plastic waste exceeds efforts to mitigate plastic pollution. *Science* **2020**, *369*, 1515−1518.
(4) Jambeck, J. R.; Geyer, R.; Wilcox, C.; Siegler, T. R.; Perryman, M.; Andrady, A.; Narayan, R.; Law, K. L. Plastic waste inputs from land into the ocean. *Science* **2015**, *347*, 768−771.
(5) Stegmann, P.; Daioglou, V.; Londo, M.; van Vuuren, D. P.; Junginger, M. Plastic futures and their CO2 emissions. *Nature* **2022**, *612*, 272−276.
(6) Nicholson, S. R.; Rorrer, N. A.; Carpenter, A. C.; Beckham, G. T. Manufacturing energy and greenhouse gas emissions associated with plastics consumption. *Joule* **2021**, *5*, 673−686.
(7) Hong, M.; Chen, E. Y.-X. Chemically recyclable polymers: a circular economy approach to sustainability. *Green Chem.* **2017**, *19*, 3692−3706.
(8) Coates, G. W.; Getzler, Y. D. Y. L. Chemical recycling to monomer for an ideal, circular polymer economy. *Nat. Rev. Mater.* **2020**, *5*, 501−516.
(9) Hong, M.; Chen, E. Y.-X. Future Directions for Sustainable Polymers. *Trends Chem.* **2019**, *1*, 148−151.
(10) Shi, C.; Reilly, L. T.; Phani Kumar, V. S.; Coile, M. W.; Nicholson, S. R.; Broadbelt, L. J.; Beckham, G. T.; Chen, E. Y.-X. Design principles for intrinsically circular polymers with tunable properties. *Chem.* **2021**, *7*, 2896−2912.
(11) Rahimi, A.; Garcia, J. M. Chemical recycling of waste plastics for new materials production. *Nat. Rev. Chem.* **2017**, *1*, 0046.
(12) Lu, X. B.; Liu, Y.; Zhou, H. Learning Nature: Recyclable Monomers and Polymers. *Chem.—Eur. J.* **2018**, *24*, 11255−11266.
(13) Tang, X.; Chen, E. Y.-X. Toward Infinitely Recyclable Plastics Derived from Renewable Cyclic Esters. *Chem.* **2019**, *5*, 284−312.
(14) Westlie, A. H.; Chen, E. Y.; Holland, C. M.; Stahl, S. S.; Doyle, M.; Trenor, S. R.; Knauer, K. M. Polyolefin Innovations toward Circularity and Sustainable Alternatives. *Macromol. Rapid Commun.* **2022**, *43*, e2200492.
(15) Worch, J. C.; Dove, A. P. 100th Anniversary of Macromolecular Science Viewpoint: Toward Catalytic Chemical Recycling of Waste (and Future) Plastics. *ACS Macro Lett.* **2020**, *9*, 1494−1506.
(16) Liu, Y.; Lu, X. B. Emerging Trends in Closed-Loop Recycling Polymers: Monomer Design and Catalytic Bulk Depolymerization. *Chem.—Eur. J.* **2023**, *29*, e202203635.
(17) Jehanno, C.; Alty, J. W.; Roosen, M.; De Meester, S.; Dove, A. P.; Chen, E. Y.-X.; Leibfarth, F. A.; Sardon, H. Critical advances and future opportunities in upcycling commodity polymers. *Nature* **2022**, *603*, 803−814.
(18) Ellis, L. D.; Rorrer, N. A.; Sullivan, K. P.; Otto, M.; McGeehan, J. E.; Román-Leshkov, Y.; Wierckx, N.; Beckham, G. T. Chemical and biological catalysis for plastics recycling and upcycling. *Nat. Catal.* **2021**, *4*, 539−556.
(19) Matyjaszewski, K. Architecturally Complex Polymers with Controlled Heterogeneity. *Science* **2011**, *333*, 1104−1105.
(20) Bates, F. S.; Hillmyer, M. A.; Lodge, T. P.; Bates, C. M.; Delaney, K. T.; Fredrickson, G. H. Multiblock polymers: panacea or Pandora's box? *Science* **2012**, *336*, 434−440.
(21) Hadjichristidis, N.; Pitsikalis, M.; Pispas, S.; Iatrou, H. Polymers with Complex Architecture by Living Anionic Polymerization. *Chem. Rev.* **2001**, *101*, 3747−3792.
(22) Guan, Z.; Cotts, P. M.; McCord, E. F.; McLain, S. J. Chain Walking: A New Strategy to Control Polymer Topology. *Science* **1999**, *283*, 2059−2062.
(23) Scheutz, G. M.; Lessard, J. J.; Sims, M. B.; Sumerlin, B. S. Adaptable crosslinks in polymeric materials: Resolving the intersection of thermoplastics and thermosets. *J. Am. Chem. Soc.* **2019**, *141*, 16181−16196.
(24) Garcia, J. M.; Jones, G. O.; Virwani, K.; McCloskey, B. D.; Boday, D. J.; ter Huurne, G. M.; Horn, H. W.; Coady, D. J.; Bintaleb, A. M.; Alabdulrahman, A. M. S.; Alsewailem, F.; Almegren, H. A. A.; Hedrick, J. L. Recyclable, strong thermosets and organogels via paraformaldehyde condensation with diamines. *Science* **2014**, *344*, 732−735.
(25) Feng, C.; Li, Y.; Yang, D.; Hu, J.; Zhang, X.; Huang, X. Well-defined graft copolymers: from controlled synthesis to multipurpose applications. *Chem. Soc. Rev.* **2011**, *40*, 1282−1295.
(26) Seo, S. E.; Hawker, C. J. The Beauty of Branching in Polymer Science. *Macromolecules* **2020**, *53*, 3257−3261.
(27) Tezuka, Y.; Oike, H. Topological polymer chemistry. *Prog. Polym. Sci.* **2002**, *27*, 1069−1122.
(28) Haque, F. M.; Grayson, S. M. The synthesis, properties and potential applications of cyclic polymers. *Nat. Chem.* **2020**, *12*, 433−444.
(29) Chang, Y. A.; Waymouth, R. M. Recent progress on the synthesis of cyclic polymers via ring-expansion strategies. *J. Polym. Sci., Part A: Polym. Chem.* **2017**, *55*, 2892−2902.
(30) Gao, C.; Yan, D. Hyperbranched polymers: from synthesis to applications. *Prog. Polym. Sci.* **2004**, *29*, 183−275.
(31) Jikei, M.; Kakimoto, M.-a. Hyperbranched polymers: a promising new class of materials. *Prog. Polym. Sci.* **2001**, *26*, 1233−1285.
(32) Voit, B. I.; Lederer, A. Hyperbranched and Highly Branched Polymer Architectures—Synthetic Strategies and Major Characterization Aspects. *Chem. Rev.* **2009**, *109*, 5924−5973.
(33) Zheng, Y.; Li, S.; Weng, Z.; Gao, C. Hyperbranched polymers: advances from synthesis to applications. *Chem. Soc. Rev.* **2015**, *44*, 4091−4130.
(34) Wu, W.; Tang, R.; Li, Q.; Li, Z. Functional hyperbranched polymers with advanced optical, electrical and magnetic properties. *Chem. Soc. Rev.* **2015**, *44*, 3997−4022.
(35) Wang, D.; Zhao, T.; Zhu, X.; Yan, D.; Wang, W. Bioapplications of hyperbranched polymers. *Chem. Soc. Rev.* **2015**, *44*, 4023−4071.
(36) Jiang, W.; Zhou, Y.; Yan, D. Hyperbranched polymer vesicles: from self-assembly, characterization, mechanisms, and properties to applications. *Chem. Soc. Rev.* **2015**, *44*, 3874−3889.
(37) Shi, C.; Zhang, Z.; Scoti, M.; Yan, X.-Y.; Chen, E. Y.-X. Endowing Polythioester Vitrimer with Intrinsic Crystallinity and Chemical Recyclability. *ChemSusChem* **2023**, *16*, e202300008.
(38) Christensen, P. R.; Scheuermann, A. M.; Loeffler, K. E.; Helms, B. A. Closed-loop recycling of plastics enabled by dynamic covalent diketoenamine bonds. *Nat. Chem.* **2019**, *11*, 442−448.
(39) Shieh, P.; Zhang, W.; Husted, K. E. L.; Kristufek, S. L.; Xiong, B.; Lundberg, D. J.; Lem, J.; Veysset, D.; Sun, Y.; Nelson, K. A.; Plata, D. L.; Johnson, J. A. Cleavable comonomers enable degradable, recyclable thermoset plastics. *Nature* **2020**, *583*, 542−547.
(40) Scheutz, G. M.; Lessard, J. J.; Sims, M. B.; Sumerlin, B. S. Adaptable crosslinks in polymeric materials: Resolving the intersection of thermoplastics and thermosets. *J. Am. Chem. Soc.* **2019**, *141*, 16181−16196.
(41) Sunder, A.; Hanselmann, R.; Frey, H.; Mülhaupt, R. Controlled Synthesis of Hyperbranched Polyglycerols by Ring-Opening Multibranching Polymerization. *Macromolecules* **1999**, *32*, 4240−4246.
(42) Lu, Y.; Nemoto, T.; Tosaka, M.; Yamago, S. Synthesis of structurally controlled hyperbranched polymers using a monomer having hierarchical reactivity. *Nat. Commun.* **2017**, *8*, 1863.
(43) Li, F.; Cao, M.; Feng, Y.; Liang, R.; Fu, X.; Zhong, M. Site-Specifically Initiated Controlled/Living Branching Radical Polymerization: A Synthetic Route toward Hierarchically Branched Architectures. *J. Am. Chem. Soc.* **2019**, *141*, 794−799.
(44) Cao, M.; Liu, Y.; Zhang, X.; Li, F.; Zhong, M. Expanding the toolbox of controlled/living branching radical polymerization through simulation-informed reaction design. *Chem.* **2022**, *8*, 1460−1475.
(45) Boas, U.; Heegaard, P. M. H. Dendrimers in drug research. *Chem. Soc. Rev.* **2004**, *33*, 43−63.

https://doi.org/10.1021/jacs.4c00526
J. Am. Chem. Soc. 2024, 146, 9261−9271

(46) Kesharwani, P.; Jain, K.; Jain, N. K. Dendrimer as nanocarrier for drug delivery. *Prog. Polym. Sci.* **2014**, *39*, 268−307.
(47) Xue, Y.; Cao, M.; Chen, C.; Zhong, M. Design of Microstructure-Engineered Polymers for Energy and Environmental Conservation. *JACS Au* **2023**, *3*, 1284−1300.
(48) Neary, W. J.; Isais, T. A.; Kennemur, J. G. Depolymerization of Bottlebrush Polypentenamers and Their Macromolecular Metamorphosis. *J. Am. Chem. Soc.* **2019**, *141*, 14220−14229.
(49) Wang, Z.; Yoon, S.; Wang, J. Breaking the Paradox between Grafting-Through and Depolymerization to Access Recyclable Graft Polymers. *Macromolecules* **2022**, *55*, 9249−9256.
(50) Quinn, E. C.; Knauer, K. M.; Beckham, G. T.; Chen, E. Y.-X. Mono-material product design with bio-based, circular, and biodegradable polymers. *One Earth* **2023**, *6*, 582−586.
(51) Shi, C.; Li, Z.-C.; Caporaso, L.; Cavallo, L.; Falivene, L.; Chen, E. Y.-X. Hybrid monomer design for unifying conflicting polymerizability, recyclability, and performance properties. *Chem.* **2021**, *7*, 670−685.
(52) Shi, C.; Clarke, R. W.; McGraw, M. L.; Chen, E. Y.-X. Closing the "One Monomer-Two Polymers-One Monomer" Loop via Orthogonal (De)polymerization of a Lactone/Olefin Hybrid. *J. Am. Chem. Soc.* **2022**, *144*, 2264−2275.
(53) Shi, C.; Reilly, L. T.; Chen, E. Y.-X. Hybrid Monomer Design Synergizing Property Trade-offs in Developing Polymers for Circularity and Performance. *Angew. Chem., Int. Ed.* **2023**, *62*, e202301850.
(54) Pratt, R. C.; Lohmeijer, B. G. G.; Long, D. A.; Waymouth, R. M.; Hedrick, J. L. Triazabicyclodecene: A Simple Bifunctional Organocatalyst for Acyl Transfer and Ring-Opening Polymerization of Cyclic Esters. *J. Am. Chem. Soc.* **2006**, *128*, 4556−4557.
(55) Chuma, A.; Horn, H. W.; Swope, W. C.; Pratt, R. C.; Zhang, L.; Lohmeijer, B. G. G.; Wade, C. G.; Waymouth, R. M.; Hedrick, J. L.; Rice, J. E. The Reaction Mechanism for the Organocatalytic Ring-Opening Polymerization of l-Lactide Using a Guanidine-Based Catalyst: Hydrogen-Bonded or Covalently Bound? *J. Am. Chem. Soc.* **2008**, *130*, 6749−6754.
(56) Hölter, D.; Burgath, A.; Frey, H. Degree of branching in hyperbranched polymers. *Acta Polym.* **1997**, *48*, 30−35.
(57) Yan, D.; Müller, A. H. E.; Matyjaszewski, K. Molecular Parameters of Hyperbranched Polymers Made by Self-Condensing Vinyl Polymerization. 2. Degree of Branching. *Macromolecules* **1997**, *30*, 7024−7033.
(58) Weigend, F.; Ahlrichs, R. Balanced basis sets of split valence, triple zeta valence and quadruple zeta valence quality for H to Rn: Design and assessment of accuracy. *Phys. Chem. Chem. Phys.* **2005**, *7*, 3297−3305.
(59) Zhao, Y.; Truhlar, D. G. The M06 suite of density functionals for main group thermochemistry, thermochemical kinetics, noncovalent interactions, excited states, and transition elements: two new functionals and systematic testing of four M06-class functionals and 12 other functionals. *Theor. Chem. Acc.* **2008**, *120*, 215−241.
(60) Grimme, S.; Antony, J.; Ehrlich, S.; Krieg, H. A consistent and accurate ab initio parametrization of density functional dispersion correction (DFT-D) for the 94 elements H-Pu. *J. Chem. Phys.* **2010**, *132*, 154104.
(61) Simón, L.; Goodman, J. M. The Mechanism of TBD-Catalyzed Ring-Opening Polymerization of Cyclic Esters. *J. Org. Chem.* **2007**, *72*, 9656−9662.
(62) Chuma, A.; Horn, H. W.; Swope, W. C.; Pratt, R. C.; Zhang, L.; Lohmeijer, B. G. G.; Wade, C. G.; Waymouth, R. M.; Hedrick, J. L.; Rice, J. E. The Reaction Mechanism for the Organocatalytic Ring-Opening Polymerization of l-Lactide Using a Guanidine-Based Catalyst: Hydrogen-Bonded or Covalently Bound? *J. Am. Chem. Soc.* **2008**, *130*, 6749−6754.
(63) Kwei, T. K. The effect of hydrogen bonding on the glass transition temperatures of polymer mixtures. *J. Polym. Sci. B Polym. Lett. Ed.* **1984**, *22*, 307−313.
(64) Lieberzeit, P.; Bekchanov, D.; Mukhamediev, M. Polyvinyl chloride modifications, properties, and applications: Review. *Polym. Adv. Technol.* **2022**, *33*, 1809−1820.
(65) Safarpour, M.; Safikhani, A.; Vatanpour, V. Polyvinyl chloride-based membranes: A review on fabrication techniques, applications and future perspectives. *Sep. Purif. Technol.* **2021**, *279*, 119678.
(66) Liu, F.; Xu, K.; Chen, M.; Cao, D. The Rheological and Mechanical Properties of PVC-Lignin Blends. *Int. Polym. Process.* **2012**, *27*, 121−127.
(67) Feldman, D.; Banu, D. Contribution to the study of rigid PVC polyblends with different lignins. *J. Appl. Polym. Sci.* **1997**, *66*, 1731−1744.

https://doi.org/10.1021/jacs.4c00526
J. Am. Chem. Soc. 2024, 146, 9261−9271